JPP Journal of Pharmacy and Pharmacology

JPP 2007, 59: 261–269

Received January 20, 2006
Accepted April 13, 2006
DOI 10.1211/jpp.59.2.0012
ISSN 0022-3573

# A theoretical and spectroscopic study of $\gamma$-crystalline and amorphous indometacin

Clare J. Strachan, Thomas Rades and Keith C. Gordon

## Abstract

Amorphous materials are prevalent in the pharmaceutical setting. Whether they are a help or hindrance, their physico-chemical characteristics must be investigated. However, the amorphous form remains a challenge to characterise with many of its properties poorly understood. In this study, $\gamma$-crystalline and amorphous indometacin are investigated using vibrational spectroscopy and quantum chemical calculations. The structure of the single indometacin molecule and the dimer in the $\gamma$-form were optimised using density functional theory calculations. The optimised structures were similar to the conformations in the crystal form, suggesting that conformation of the molecules in the crystal may be close to the average molecular structure in less-ordered states. Infrared and Raman spectra were calculated from the optimised structures. Many modes in the calculated spectra could be matched with the experimental spectra of the $\gamma$-crystalline and amorphous forms, and a description of the matched modes has been provided. By analysis of the theoretical vibrational modes it was confirmed that the amorphous form of indometacin produced by quench cooling the melt consists predominantly of dimers, similar in structure to in the $\gamma$-crystalline form. In addition, differences in intermolecular bonding between the two forms were identified. Quantum mechanical calculations allow improved understanding of amorphous materials and their vibrational spectra.

## Introduction

Molecular solids can be divided into three broad categories according to their degree of molecular long-range orientational and positional order. Crystal structures possess orientational and positional long-range order in all three dimensions in space. Liquid crystalline forms are less ordered and contain long-range orientational and positional order in one or two dimensions, but not all three dimensions. A third form possible in the solid state is the amorphous form. Amorphous materials may contain short-range orientational and positional order (e.g., due to the formation of molecular dimers) but not long-range order (Brittain 2000; Bernstein 2002; Bunjes & Rades 2005).

Amorphous solids can exist as a rubbery state and, at lower temperatures, as a glassy state. The molecular mobility in the rubbery state is higher than in the glassy state, and the $T_g$ represents the temperature at which the material cannot kinetically obtain equilibrium as thermal energy is removed from the system (Forster 2001; Hancock 2002). Depending on the method of preparation the temperature of the $T_g$ can change and kinetic states, relaxation times and glass properties may also be altered (Forster 2001). Despite progress in thermodynamic and kinetic analysis of amorphous solids, many properties of the amorphous form remain poorly understood.

The amorphous form has been of particular interest to the pharmaceutical industry because materials in this state exhibit enhanced dissolution rates and solubility compared with their crystalline counterparts (Hancock & Parks 2000). However, even in the glassy state, the amorphous form is prone to solid-state conversions to more thermodynamically favourable forms. In addition, properties of the amorphous form depend on the method of preparation, and the question of polyamorphism or discrete amorphous forms is currently under debate. These issues have, at least in part, hindered the adoption of the amorphous form for use in commercial dosage forms.

School of Pharmacy, University of Otago, Dunedin, New Zealand

Clare J. Strachan, Thomas Rades

Division of Pharmaceutical Technology, Faculty of Pharmacy, University of Helsinki, Finland

Clare J. Strachan

Drug Discovery and Development Technology Centre (DDTC), Faculty of Pharmacy, University of Helsinki, Finland

Clare J. Strachan

Department of Chemistry, University of Otago, Dunedin, New Zealand

Keith C. Gordon

**Correspondence:** K. C. Gordon, Department of Chemistry, University of Otago, Dunedin, New Zealand. E-mail: kgordon@chemistry.otago.ac.nz

The amorphous form poses a significant challenge for structural analysis. Little information can be gained from X-ray diffraction, which probes the lattice level. Techniques that probe the molecular level, such as vibrational spectroscopy may provide more insight into amorphous systems. Quantum chemical modelling is one approach that could be used to improve understanding of the amorphous form. Quantum chemical analysis of pharmaceutical drugs has not been widely investigated. Some studies have been undertaken investigating conformational stability to increase understanding of drug–receptor interactions and drug metabolism pathways (Kubli-Garfias 1998, 1999). Ranitidine hydrochloride has been investigated in relation to crystallographic data (Martins et al 2002), but there are few studies involving drug polymorphism and prediction of vibrational spectra of drug polymorphs (Strachan et al 2004).

Indometacin is an indole acetic acid derivative used as a non-steroidal anti-inflammatory agent. It is practically insoluble in water and can be classified as a Class II drug in the Biopharmaceutical Classification System (Amidon et al 1995; US Department of Health and Human Services 2000). It is polymorphic, with three forms having been reported (Crowley & Zografi 2002a). The $\gamma$-form, the stable form at room temperature, is triclinic with space group, $P\bar{1}$ (Kirstenmacher & Marsh 1972; Galdecki & Glówka 1976).

In the amorphous form, indometacin exhibits significantly enhanced dissolution (Hancock & Parks 2000). The amorphous form can be easily produced, without significant degradation, by melting and subsequent cooling. Indometacin has been used as a model compound for investigation and development of amorphous drug formulations (Forster et al 2001a, b, c; Tong & Zografi 2001; Watanabe et al 2001, 2002, 2003; Crowley & Zografi 2002b, 2003; Fini et al 2002). In a study by Taylor & Zografi (1997), quench-cooled amorphous indometacin and molecular dispersions of indometacin were prepared, and, by comparing their vibrational spectra, it was deduced that amorphous indometacin exists predominantly as dimers.

In this study, quantum chemical calculations are used to predict vibrational spectra (infrared (IR) and Raman) of indometacin. These spectra are compared with experimental vibrational spectra of $\gamma$-crystalline and amorphous indometacin allowing improved analysis of the vibrational spectra and structural interpretation of amorphous indometacin.

## Materials and Methods

### Materials

Indometacin (Figure 1) was purchased from Sigma Chemical Co. (CAS 53-86-1; St Louis, MO, USA). The $\gamma$-crystalline form was used as supplied. Amorphous samples were produced by the method described by Taylor & Zografi (1997). Indometacin was melted on a stainless-steel plate at 165°C in an oven for 5 min and quench-cooled using liquid nitrogen. The amorphous material was warmed to room temperature under vacuum to prevent atmospheric moisture condensation on the sample. The amorphous material was then ground in a mortar and pestle, stored at 4°C over silica gel, and analysed not more than 24 h after preparation. The solid-state forms were verified by X-ray powder diffractometry (PANalytical X'Pert PRO MPD system, Holland).

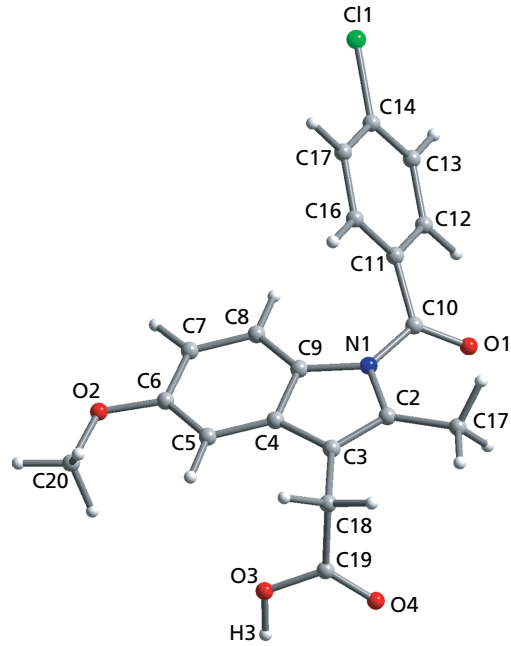


**Figure 1** Molecular structure of indometacin with atomic numbering. The numbering system follows that used by Kirstenmacher & Marsh (1972).

### Spectroscopy

IR spectroscopy was performed using a Fourier transform IR (FTIR) spectrometer (FTS 175C; BioRad Laboratories, MA, USA) with a diffuse reflectance accessory attached (Pike Technology Easidiff, Madison, WI, USA). Samples (5%) in anhydrous potassium bromide (250 mg total) were ground gently for 2 min in a mortar and pestle, placed in the sample holder and the surface smoothed with a blade. Anhydrous potassium bromide subjected to the same sample treatment was used to record a reference spectrum. Spectra were recorded after Kubelka-Munk transformation, and were the mean of 32 scans with a resolution of 4 $cm^{-1}$.

FT-Raman spectroscopy was carried out on powder samples using a Bruker IFS 55 interferometer fitted with a Bruker FRA 106 S FT-Raman accessory. The instrument used a D 425 Ge diode detector and a Compass 1064–500 laser. Analysis was carried out at room temperature with a laser wavelength of 1064 nm and 105 mW power. Samples were packed in an aluminium sample holder and spectra were collected at a resolution of 4 $cm^{-1}$. Spectra were the average of 150 scans. All spectra were analysed using GRAMSAI software (Galactic Industries, Salem, NH, USA).

### Computational studies

Quantum chemical modelling was performed on the indometacin single molecule and the dimer structure that exists in the $\gamma$-crystalline form. The molecular conformation

of γ-crystalline indometacin published by Kirstenmacher & Marsh (1972) was obtained from the Cambridge Crystallographic Database (CCDC, Cambridge, UK) using Conquest software and used as a starting point for the single molecule calculations. For the dimer calculations, the single molecule provided by Kirstenmacher & Marsh (1972) was duplicated and adjusted to resemble the dimer conformation in the γ-form.

Optimised molecular conformations followed by their vibrational frequencies and their IR and Raman intensities were calculated using density functional theory (DFT) calculations (B3LYP functional, 6-31G(d) basis set). Calculations were implemented using the Gaussian 03 program (Frisch et al 2004). The Raman intensities were calculated from the Raman activity for 1064 nm excitation (Guirgis et al 2000). The calculated frequencies were scaled by a factor of 0.9682 (Scott & Radom 1996), which was obtained by taking the least squares difference between the scaled theoretical and experimental wavenumbers between 1000 and 1800 $cm^{-1}$ and minimising this difference by variation of the scaling factor. Modes were visualised using the GaussView package that accompanies Gaussian 03 and Molden (Schaftenaar & Noordik 2000).

## Results and Discussion

### Conformational analysis

Kirstenmacher & Marsh (1972) and Galdecki & Glówka (1976) have carried out structural studies on the γ-form of indometacin. Bond lengths, angles and dihedral angles (and their standard deviations (s.d.)) obtained by both groups are presented in Table 1, and the numbering system used is depicted in Figure 1. In the γ-form, indometacin molecules are associated as dimers, with cyclic hydrogen bonding between the carboxylic acid groups (Figure 2A). There are no significant differences (within 3 s.d.) between the structures determined by Kirstenmacher & Marsh (1972) and Galdecki & Glówka (Galdecki & Glówka 1976). Therefore, the experimentally determined structural parameters mentioned henceforth will be those of Kirstenmacher & Marsh.

Bond lengths, angles and dihedral angles of the single molecule and dimer after optimisation are also presented in Table 1. Most of the bond lengths and angles in the single molecule were virtually identical to those in the dimer (notable differences shown in Table 1). The only differences were associated with the carboxylic acid moiety, from which cyclic hydrogen bonding occurs in the dimer structure. Not surprisingly, the geometry of this moiety in the γ-crystalline form was more closely replicated in the optimised dimer than in the single molecule. In particular, the C19-O3 bond measures 1.299 Å in the crystal structure, and was 1.357 and 1.323 Å in the single molecule and dimer, respectively. The C18-C19-O4 angle (122.9° in the crystal form) was 125.5° in the single molecule and 122.1° in the dimer, and the C18-C19-O3 angle (113.9° in the crystal form) measured 111.7 and 113.4° in the single molecule and dimer, respectively.

Intermolecular distances and angles associated with the hydrogen bonding of the carboxylic acid groups in the dimer and crystal structure are documented in Table 2. The O3(a)-O4(b) bond is longer in the optimised dimer (2.683 Å) than in the crystal form (2.669 Å), and the C19(a)-O3(a)-O4(b)-C19(b) dihedral angle smaller in the optimised dimer (−1.8°) than in the γ-form (−6.2°).

The conformation of the *p*-chlorophenyl ring and the neighbouring carbonyl group in relation to the indole group has been discussed by Kirstenmacher & Marsh (1972). The angle of the carbonyl group to the indole group was closely replicated in the optimised single molecule (and dimer), with the C2-N1-C10-O1 dihedral angle −25.5° and −29.6° in the crystal structure and optimised single molecule, respectively. The angle between the *p*-chlorophenyl ring and the carbonyl group was somewhat smaller in the optimised structure (−28.8° in the single molecule) than in the crystal structure (−39.3°).

The two molecules in the optimised dimer have different, but energetically equivalent, conformations with inversion symmetry about point P (Figure 2A). Thus, the carboxyl moiety has been reflected in the plane of the indole group, so that the C2-C3-C18-C19 dihedral angle in the dimer is 97.6° in molecule A and −97.6° in molecule B (Table 1). In addition, the chlorophenyl and carbonyl groups in molecule B are reflected in the indole group plane, such that the C2-N1-C10-O1 dihedral angle is −29.3° in molecule A and 29.3° in molecule B. For these and the other modifications in molecule B to be accommodated during crystallisation, several single bond rotations must occur. Energetically equivalent conformational differences have also been observed in the dimers in form III (p-monoclinic) of carbamazepine (Strachan et al 2004).

Overall, the geometry of the optimised single molecule and dimer are similar to that in those in the γ-crystalline form of indometacin. This suggests that the conformation present in the crystal structure is close to the lowest energy conformation of the single molecule. Large differences were, however, observed with many dihedral angles. This can be explained by the low energy associated with single bond rotations. It is single bonds that are most easily rotated when a molecule is accommodated into a crystal structure. The optimised single molecule and dimer are, therefore, suitable structures for the calculation of vibrational spectra of indometacin to improve understanding of indometacin, and especially amorphous indometacin, in the solid state.

### Spectroscopic analysis

Experimental IR and Raman spectra of γ-crystalline and amorphous indometacin have been discussed by Taylor & Zografi (1997, 1998). Both the IR and Raman spectra of amorphous indometacin exhibit broader, less intense peaks than those of the γ-crystalline form (Figures 3, 4 and 5). This can be attributed to a range of molecular conformations and intermolecular bonding arrangements in the amorphous form. In addition, there are some spectral shifts between the amorphous and γ-crystalline forms, particularly for some bands that are IR active.

**Table 1** Bond lengths, angles and dihedral angles from the literature and after optimisation

| **Bond parameters** | **γ-Crystal form** | | |
|---|---|---|---|
| | Kirstenmacher & Marsh (1972) | Galdecki & Glówka (1976) | Calculated B3LYP 6–31G(d) |
| *r* | | | |
| N1-C2 | 1.416 (5) | 1.399 (28) | 1.414 |
| C2-C3 | 1.354 (5) | 1.371 (81) | 1.371 |
| C3-C4 | 1.433 (5) | 1.436 (38) | 1.444 |
| C4-C5 | 1.401 (5) | 1.419 (100) | 1.405 |
| C5-C6 | 1.375 (5) | 1.365 (22) | 1.393 |
| C6-C7 | 1.404 (5) | 1.423 (41) | 1.411 |
| C7-C8 | 1.379 (5) | 1.398 (98) | 1.388 |
| C8-C9 | 1.386 (5) | 1.391 (24) | 1.399 |
| C9-C4 | 1.401 (5) | 1.395 (40) | 1.410 |
| C9-N1 | 1.416 (5) | 1.417 (93) | 1.416 |
| N1-C10 | 1.416 (5) | 1.415 (59) | 1.413 |
| C10-C11 | 1.485 (5) | 1.489 (27) | 1.495 |
| C11-C12 | 1.393 (5) | 1.402 (21) | 1.402 |
| C12-C13 | 1.379 (5) | 1.412 (28) | 1.391 |
| C13-C14 | 1.373 (5) | 1.370 (25) | 1.396 |
| C14-C15 | 1.381 (5) | 1.390 (20) | 1.395 |
| C15-C16 | 1.375 (5) | 1.361 (27) | 1.393 |
| C16-C11 | 1.389 (5) | 1.389 (26) | 1.402 |
| C14-Cl1 | 1.735 (5) | 1.768 (35) | 1.754 |
| C10-O1 | 1.207 (5) | 1.207 (46) | 1.220 |
| C2-C17 | 1.480 (5) | 1.516 (82) | 1.495 |
| C3-C18 | 1.493 (5) | 1.492 (37) | 1.508 |
| C18-C19 | 1.501 (5) | 1.478 (16) | 1.520 |
| C19-O3 | 1.299 (5) | 1.302 (51) | 1.357 (1.323) |
| C19-04 | 1.212 (5) | 1.232 (16) | 1.210 (1.230) |
| 03-H3 | 1.07 (3) | No data | 0.976 |
| C6-O2 | 1.376 (5) | 1.395 (96) | 1.368 |
| 02-C20 | 1.419 (5) | 1.430 (47) | 1.417 |
| *θ* | | | |
| C9-N1-C2 | 108.1 (4) | 108.4 (5) | 108.2 |
| N1-C2-C3 | 108.5 (4) | 109.2 (5) | 108.8 |
| C2-C3-C4 | 108.7 (4) | 107.2 (3) | 108.1 |
| C3-C4-C9 | 107.6 (4) | 108.6 (2) | 107.4 |
| C4-C9-N1 | 107.0 (4) | 106.6 (4) | 107.3 |
| C8-C9-N4 | 120.8 (4) | 121.3 (2) | 120.8 |
| C9-C4-C5 | 121.0 (4) | 121.4 (4) | 120.6 |
| C4-C5-C6 | 117.9 (4) | 117.1 (4) | 118.4 |
| C5-C6-C7 | 120.7 (4) | 121.9 (2) | 120.5 |
| C6-C7-C8 | 121.8 (4) | 120.7 (3) | 121.4 |
| C7-C8-C9 | 117.8 (4) | 117.5 (4) | 118.2 |
| C7-C6-O2 | 114.3 (4) | 113.1 (4) | 114.9 |
| 02-C6-C5 | 125.0 (4) | 125.0 (4) | 124.6 |
| C6-O2-C20 | 117.9 (4) | 117.1 (4) | 118.0 |
| C3-C4-C5 | 131.4 (4) | 130.0 (4) | 131.9 |
| C4-C3-C18 | 123.7 (4) | 124.0 (3) | 125.4 (125.1) |
| C2-C3-C18 | 127.6 (4) | 128.9 (4) | 126.5 |
| C3-C2-C17 | 128.9 (4) | 128.2 (2) | 128.6 |
| N1-C2-C17 | 122.4 (4) | 122.5 (4) | 122.5 |
| N1-C9-C8 | 132.1 (4) | 132.0 (5) | 131.7 |
| C3-C18-C19 | 112.5 (4) | 112.4 (2) | 111.4 |
| C18-C19-O4 | 122.9 (4) | 123.0 (2) | 125.5 (122.1) |
| C18-C19-O3 | 113.9 (4) | 115.1 (3) | 111.7 (113.4) |
| O3-C19-O4 | 123.1 (4) | 121.8 (3) | 122.8 |
| C19-O3-H3 | 110.0 (10)* | No data | 106.1 (110.2) |
| C9-N1-C10 | 126.7 (4) | 126.5 (2) | 127.5 |
| C2-N1-C10 | 124.7 (4) | 124.7 (3) | 123.8 |
| N1-C10-O1 | 120.9 (4) | 121.4 (2) | 121.1 |
| N1-C10-C11 | 116.7 (4) | 116.8 (3) | 118.0 |

(*Cont.*)

**Table 1** (*Cont.*)

| Bond parameters | γ-Crystal form | | |
|---|---|---|---|
| | Kirstenmacher & Marsh (1972) | Galdecki & Glówka (1976) | Calculated B3LYP 6–31G(d) |
| O1-C10-C11 | 122.4 (4) | 121.6 (3) | 120.8 |
| C10-C11-C12 | 118.7 (4) | 117.1 (1) | 117.7 |
| C10-C11-C16 | 122.0 (4) | 122.2 (2) | 122.7 |
| C16-C11-C12 | 119.0 (4) | 120.6 (2) | 119.3 |
| C11-C12-C13 | 120.2 (4) | 118.3 (1) | 120.7 |
| C12-C13-C14 | 119.7 (4) | 118.6 (3) | 119.0 |
| C13-C14-C15 | 121.0 (4) | 123.3 (2) | 121.3 |
| C14-C15-C16 | 119.2 (4) | 117.9 (1) | 119.1 |
| C15-C16-C11 | 120.8 (4) | 121.3 (2) | 120.5 |
| C15-C14-Cl1 | 119.5 (4) | 118.6 (1) | 119.3 |
| C13-C14-Cl1 | 119.4 (4) | 118.2 (2) | 119.3 |
| $\phi$ | | | |
| C2-N1-C10-O1 | –25.5 (3) | –26.1 | –29.6 (–29.3, 29.3) |
| N1-C10-C11-C12 | 144.2 | 143.2 | 154.4 (153.9, –153.8) |
| O1-C10-C11-C12 | –39.3 (3) | –40.3 | –28.8 (–29.4, 29.5) |
| C2-C3-C18-C19 | 99.9 | 100.6 | 88.4 (97.6, –97.6) |
| C3-C18-C19-O3 | 146.7 | 147.9 | 84.7 (90.9, –91.1) |
| C3-C18-C19-O4 | –34.9 | –35.0 | –93.8 (–87.9, 87.7) |
| C5-C6-O2-C20 | 5.9 | 7.3 | 0.1 (0.7, –0.7) |

Bond lengths, $r$ (Å); bond angles, $\theta$ (°); dihedral angles, $\phi$ (°). Values in parentheses for the crystal form are the published standard deviations (corresponding to the last decimal place). Parameter values not documented were obtained from the crystal conformation in Conquest, in which case no standard deviations were obtained. Values in parentheses for the calculated conformation are optimised γ-crystalline form values calculated from the dimer that are substantially different from the optimised values calculated from the monomer. Values after a comma in the parentheses are values for molecule B, when they are substantially different to those for molecule A. Computational method used was B3LYP and 6-31G was the basis set used in optimisation. *Measured using Mercury Software (2001).

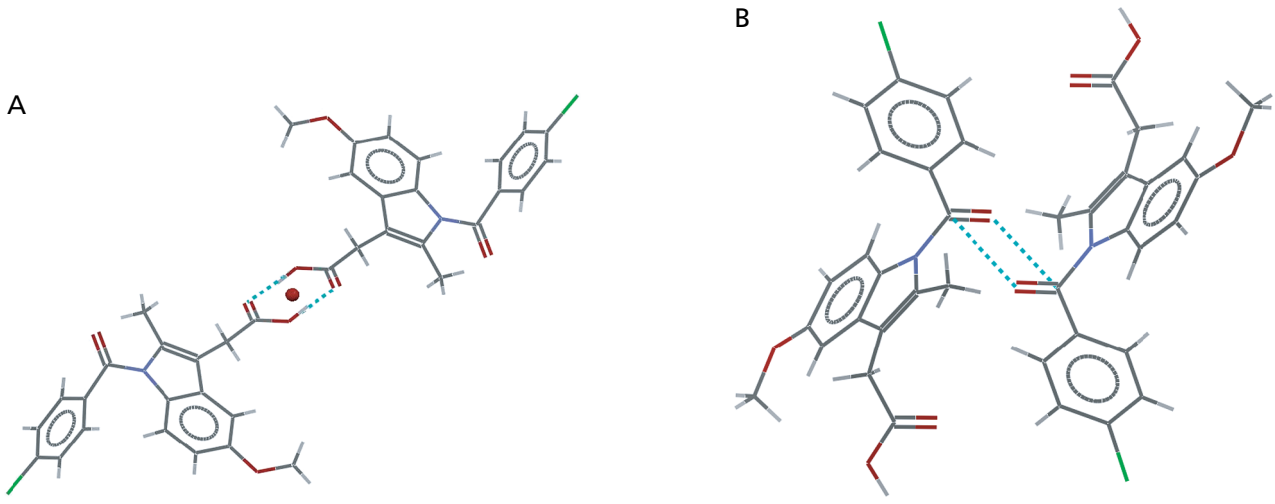


**Figure 2** Structure of γ-crystalline indometacin (A) dimer structure with hydrogen bonding between the carboxylic acid groups and point P of inversion symmetry (red circle). B. Intermolecular bonding between the benzoyl groups of adjacent molecules.

The IR and Raman spectra of the optimised monomer and dimer were calculated and compared with the experimental spectra of γ-crystalline and amorphous indometacin (Figures 3, 4 and 5). Several calculated modes have been matched with experimentally observed bands in the IR and Raman spectra, and these modes have been described (Table 3).

The experimental spectra show polymorph sensitive modes in the 1700 $cm^{-1}$ region. The single molecule indometacin calculation predicts a mode at 1705 $cm^{-1}$ ($\nu$(100)), which is both IR and Raman active (Figures 3 and 4). The mode is a benzoyl stretching vibration and occurred at 1705 $cm^{-1}$ in the dimer calculation (Figure 6B); this mode is unchanged in going from monomer to dimer as the benzoyl groups are remote from the portion of the molecule involved in the dimer formation. In the crystalline form this band appears at 1695 $cm^{-1}$, and is the most intense band in both the experimental IR and Raman spectra. In the IR spectrum of the amorphous form the band splits into two, with

**Table 2** Some parameters involving both molecules in the dimer from the literature and after optimisation

| Bond parameters | γ-Crystal form | | |
|---|---|---|---|
| | Kirstenmacher & Marsh (1972) | Galdecki & Glówka (1976) | Calculated B3LYP 6–31G(d) |
| *r* | | | |
| O3(a)-O4(b) | 2.669 | 2.664* | 2.683 |
| H3(a)-O4(b) | 1.604 | No data | 1.677 |
| *θ* | | | |
| C19(a)-O3(a)-O4(b) | 110.9* | 111.9* | 110.2 (110.7) |
| O3(a)-H3(a)-O4(b) | 174.7* | No data | 179.3 |
| *ϕ* | | | |
| O3(a)-H3(a)--O4(b)-C19(b) | 174.23 (−174.84)* | No data | 172.8 (−175.7) |
| C19(a)-O3(a)--O4(b)-C19(b) | −6.16 (6.16)* | 173.61 | −1.810 (1.651) |

See Table 1 for specifications. *Measured using Mercury Software (2001).

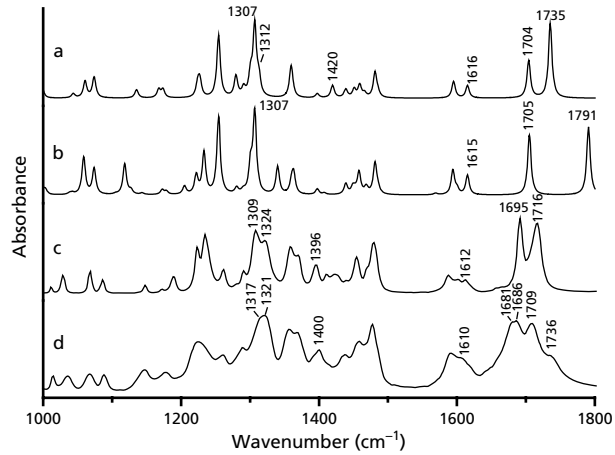


**Figure 3** IR spectra of calculated indometacin dimer (a), calculated indometacin single molecule (b), experimental crystalline indometacin (c) and experimental amorphous indometacin (d) between 1000 and 1800 $cm^{-1}$.

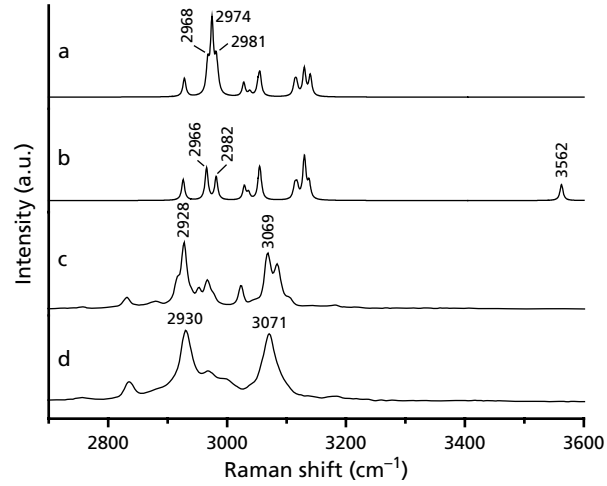


**Figure 5** Raman spectra of calculated indometacin dimer (a), calculated indometacin single molecule (b), experimental crystalline indometacin (c) and experimental amorphous indometacin (d) between 2700 and 3600 $cm^{-1}$.

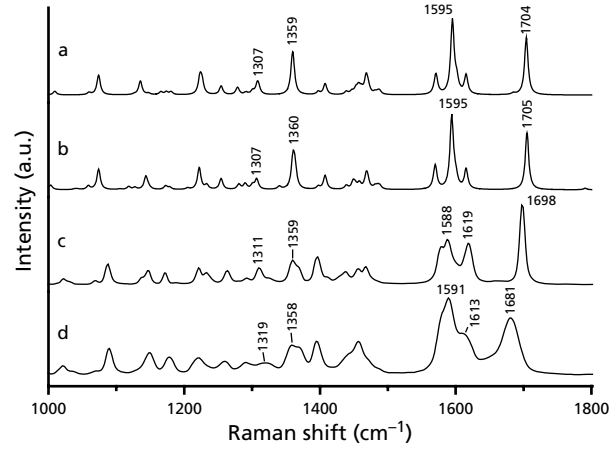


**Figure 4** Raman spectra of calculated indometacin dimer (a), calculated indometacin single molecule (b), experimental crystalline indometacin (c) and experimental amorphous indometacin (d) between 1000 and 1800 $cm^{-1}$.

maxima at 1681 and 1686 $cm^{-1}$. However, in the Raman spectrum, only the mode at 1681 $cm^{-1}$ is observed. In the γ-crystalline form the benzoyl group forms intermolecular bonds with the benzoyl group of a neighbouring molecule (Figure 2B). The intermolecular C10–O1 distance is 3.19 Å. In the amorphous form it is unlikely that the benzoyl group forms such close intermolecular associations, which may explain the higher frequency of this mode in the γ-form. The split of $\nu(100)$ into two IR-active modes in the amorphous form may be due to partial or varied intermolecular bonding of the benzoyl group (Table 4). Furthermore it should be appreciated that the dimer model used in the calculation does not model benzoyl–benzoyl interactions and thus the calculations are less effective in shedding light on the interactions of these groups in comparison with the carboxylate groups.

An IR active mode was calculated at 1791 $cm^{-1}$ for the single molecule calculation ($\nu(101)$). This mode corresponds to an asymmetric carbonyl stretch of the carboxylate group.

**Table 3** Calculated and experimental wavenumbers and intensities

| $\upsilon$ | Calculated monomer $\upsilon$ (cm)$^{-1}$ (IR, R Int) | Calculated dimer $\upsilon$ (cm$^{-1}$) (IR, R Int) | Experimental $\gamma$-crystalline $\upsilon$ (cm$^{-1}$) (IR, R Int) | Experimental amorphous $\upsilon$ (cm$^{-1}$) (IR, R Int) | Vibrational assignment |
|---|---|---|---|---|---|
| 63 | 1059 (46, 5) | 1060 (23, 3) | 1068 (29, 5) | 1069 (22, 5) | In-plane chlorobenzene ring breathing, in-plane indole deformation, C20-O2 stretching, N1-C10 stretching |
| 64 | 1074 (32, 28) | 1074 (27, 26) | 1086 (18, 26) | 1089 (21, 34) | C14-Cl stretching, in-plane chlorobenzene ring breathing |
| 73 | 1222 (23, 30) | 1224 (18, 22) | 1223 (61, 21) | 1223 (65, 22) | C10-C11 stretching, out-of-phase C6-O2-C20 stretching, out-of-phase C2-N1-C9 stretching (mainly dimer) |
| 74 | 1233 (51, 6) | 1226 (20, 17) | 1234 (78, 15) | 1233 (60, 0) | Out-of-phase C17-C2-N1 stretching, out-of-phase C6-O2-C20 stretching, in-phase O3-C19-O4 stretching (monomer only) |
| 75 | 1254 (95, 15) | 1254 (18, 22)<br>1278 (0, 10)<br>1280 (27, 0) | 1262 (32, 18) | 1261 (47, 18) | Out-of-phase C2-N1-C10 stretching (monomer) and out-of-phase N1-C10-C1 stretching (dimer), out-of-phase C6-O2-C20 stretching, in-plane indole and chlorobenzene ring deformations, C19-O3 stretching (dimer) |
| 80 | 1307 (100, 14) | 1307 (95, 14) | 1310 (84, 21) | 1318 (96, 16) | Out-of-phase and in-phase C9-N1-C10 stretching, in-plane indole and chlorobenzene ring defomrations |
| 82 | 1360 (14, 40) | 1359 (22, 24) | 1359 (62, 31) | 1358 (82, 39) | Indole ring deformation, C3-C18 stretching, C10-N1 stretching |
| 83 | 1363 (24, 26) | 1360 (20, 37) | 1369 (51, 23) | 1369 (77, 36) | Indole ring deformation, C3-C18 stretching, C10-N1 stretching |
| 85 | 1408 (2, 19) | 1407 (0, 15) | 1396 (0, 35) | 1395 (0, 44) | C2-C17 stretching, in-phase C17-$H_3$ inversion |
| 89 | 1458 (27, 8) | 1458 (18, 10) | 1455 (48, 20) | 1458 (66, 44) | In-plane indole ring deformation |
| 90 | 1468 (7, 16) | 1467 (5, 24) | 1469 (35, 23) | 1470 (n.a., 22) | In-phase C19-04-H3 bending (dimer, in phase), C18$H_2$ scissoring, C17$CH_3$ asymmetric bending |
| 92 | 1481 (38, 4) | 1482 (31, 3) | 1479 (67, 0) | 1477 (88, 0) | C6-O2 stretching, indole ring deformation |
| 96 | 1570 (1, 31) | 1571 (0, 26) | 1579 (0, 48) | 1580 (0, 80) | In-plane indole ring deformation |
| 97 | 1595 (30, 100) | 1595 (24, 100) | 1588 (24, 57) | 1591 (50, 100) | Chlorobenzyl ring deformation, C2-C3 stretching |
| 99 | 1615 (24, 27) | 1616 (19, 26) | 1612 (18, 52) (1619 for Raman) | 1610 (43, 54) (1613 for Raman) | C6-O2 stretching, indole ring deformation |
| 100 | 1705 (74, 78) | 1704 (46, 79) | 1696 (100, 100) | 1681 (92, 74)<br>1686 (93, 0) | C10-O1 stretching |
| 101 | 1791 (84, 2) | 1735 (100, 0) | 1716 (92, 0) | 1709 (89, 0) | Asymmetric O3-C19 = O4 stretching (carboxylic acids out-of-phase in dimer) |

$\upsilon$, Mode number. For experimental data, relative intensities for bands were normalised such that the most intense band in the reported spectral region is 100, n.a. = not apparent. Only calculated modes that have been matched with experimentally observed modes are shown. Where differences occur between the experimental IR and Raman spectra, the mean frequency is reported.

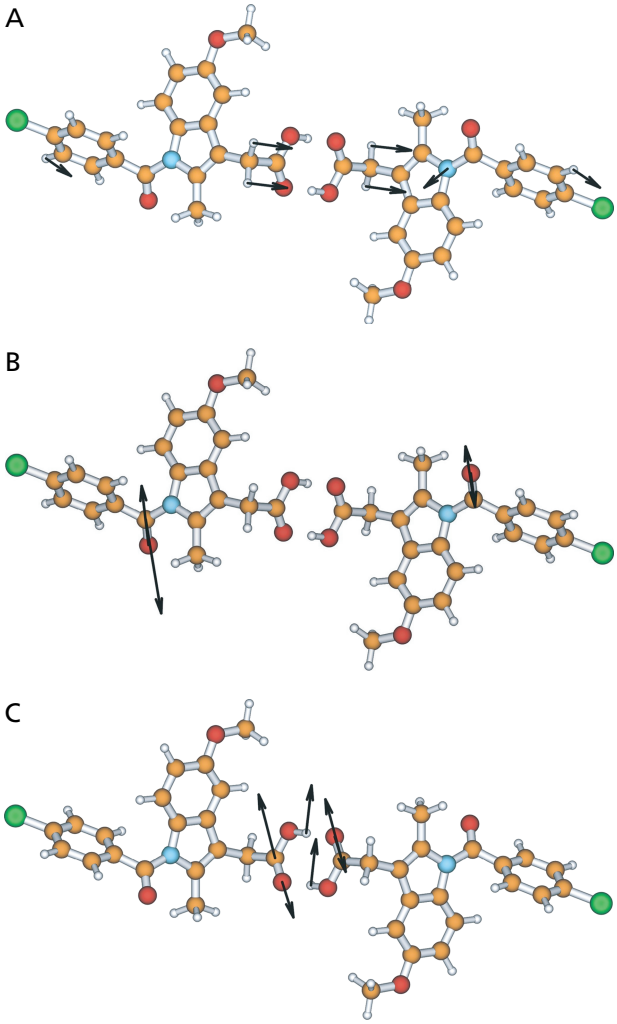


**Figure 6** Selected normal modes for indometacin dimer $\nu(80)$ (A), $\nu(100)$ (B) and $\nu(101)$ (C) from Table 3. Only the largest eigenvectors are shown for clarity.

In the dimer calculation, this mode is down-shifted by 56 $cm^{-1}$ to 1735 $cm^{-1}$. The predicted frequency for this mode in the dimer is much closer to that experimentally observed, consistent with the presence of dimers in the solid-state structure and, importantly, indicating that the calculation has correctly modelled this solid-state interaction. The mode is also somewhat modified, involving carbonyl stretches of the hydrogen-bonding carboxylate groups (Figure 6C). The dimer calculation also agrees much more closely with the mode observed in both the $\gamma$-crystalline and amorphous forms. This shows that the amorphous form is also principally composed of dimers. It is also interesting to note that the amorphous form of indometacin shows a further splitting of this band, suggesting a number of bonding domains that remain predominantly dimer in nature.

Further evidence of dimerisation in the amorphous form is found in the CH region of the Raman spectra. In the calculated spectrum of the single molecule, a band corresponding to the OH stretch in the carboxylic acid group occurs at 3562 $cm^{-1}$. This band is downshifted to 2974 $cm^{-1}$ in the dimer spectrum, and can be matched with comparatively strong bands in both the amorphous and crystalline forms at 2928 $cm^{-1}$ and 2930 $cm^{-1}$, respectively.

In a study by Taylor & Zografi (1997), IR and Raman spectroscopy were used in conjunction with molecular dispersions of indometacin in PVP to establish that quench-cooled amorphous indometacin consists predominantly of dimers. The results in our study support this finding. An advantage of our approach is that preparation of other forms such as molecular dispersions is not necessary.

It is interesting to note that the calculation of the indometacin dimer shows a number of bands that are virtually unshifted from the single molecule calculation. One such mode occurs at 1307 $cm^{-1}$ ($\nu(80)$) for both the single molecule and dimer calculations. This mode is solid-state sensitive: it occurs at 1310 $cm^{-1}$ in the $\gamma$-crystalline form, and at 1318 $cm^{-1}$ in the amorphous form. Analysis of the normal vibration shows that this mode is delocalized over much of the indometacin molecule with significant contributions for the $CH_2$ groups adjacent to the carboxylate functions (Figure 6A). In the crystalline form the mode is well defined; however in the amorphous form this mode is much broader and less intense. This is particularly noticeable in the Raman spectrum. This mode highlights that the crystalline form contains a well-defined molecular conformation, whereas the amorphous form contains a range of molecular conformations and intermolecular bonding arrangements.

## Conclusions

Density functional theory calculations were successfully employed to analyse the structure and IR and Raman spectra of indometacin. The differences in the vibrational modes of $\gamma$-crystalline and amorphous indometacin were analysed, which provided insight into the structure of amorphous indometacin. In particular, it was possible to confirm amorphous indometacin formed by quench-cooling exists predominantly as dimers.

**Table 4** Modes calculated from the dimer only and corresponding experimental wavenumbers and intensities

| $\upsilon$ | Calculated dimer $\upsilon$ $(cm)^{-1}$ (IR, R Int) | Experimental $\gamma$-crystalline $\upsilon$ $(cm)^{-1}$ (IR, R Int) | Experimental amorphous $\upsilon$ $(cm)^{-1}$ (IR, R Int) | Vibrational assignment |
|---|---|---|---|---|
| 165, 166 | 1312 (21, 6) | 1324 (70, 8) | 1321 (100, 0) | C19-O3-H1 bending (carboxylic acids out-of-phase) |
| 175 | 1420 (15, 0) | 1396 (37, 0) | 1400 (54, 0) | C19-O3-H1 bending (carboxylic acids out-of-phase) |

$\upsilon$, Mode number. For experimental data, relative intensities for bands were normalised such that the most intense band in the reported spectral region is 100, n.a. = not apparent. Only calculated modes that have been matched with experimentally observed modes are shown. Where differences occur between the experimental IR and Raman spectra, the mean frequency is reported.

Density functional calculations offer great potential to improve understanding of the structural properties of solid-state pharmaceutical materials, especially those of amorphous materials. Future work will involve using density functional calculations to investigate amorphous indometacin prepared by other methods.

## References


Amidon, G. L., Lennernäs, H., Shah, V. P., Crison, J. R. (1995) A theoretical basis for a biopharmaceutic drug classification: the correlation of in vitro drug product dissolution and in vivo bioavailability. *Pharm. Res*. **12**: 413–420

Bernstein, J. (2002) Polymorphism in molecular crystals. In: Coppens, A. A. C. (ed.) *International Union of Crystallography monographs on crystallography*. Oxford University Press, Oxford, p. 410

Brittain, H. G. (2000) *Polymorphism in pharmaceutical solids*. Marcel, Dekker Inc., New York

Bunjes, H., Rades, T. (2005) Thermotropic liquid crystalline drugs. *J. Pharm. Pharmacol*. **57**: 807–816

Crowley, K. J., Zografi, G. (2002a) Cryogenic grinding of indomethacin polymorphs and solvates: assessment of amorphous phase formation and amorphous phase physical stability. *J. Pharm. Sci*. **91**: 492–507

Crowley, K. J., Zografi, G. (2002b) Water vapor absorption into amorphous hydrophobic drug/poly(vinylpyrrolidone) dispersions. *J. Pharm. Sci*. **91**: 2150–2165

Crowley, K. J., Zografi, G. (2003) The effect of low concentrations of molecularly dispersed poly(vinylpyrrolidone) on indomethacin crystallization from the amorphous state. *Pharm. Res*. **20**: 1417–1422

Fini, A., Holgado, M. A., Rodriguez, L., Cavallari, C. (2002) Ultrasound-compacted indomethacin/polyvinylpyrrolidone systems: effect of compaction process on particle morphology and dissolution behavior. *J. Pharm. Sci*. **91**: 1880–1890

Forster, A. (2001) *An investigation of melt extrusion for the preparation of glass solutions of poorly water soluble drugs*. PhD Thesis, University of Otago, Dunedin

Forster, A., Hempenstall, J., Rades, T. (2001a) Characterization of glass solutions of poorly water-soluble drugs produced by melt extrusion with hydrophilic amorphous polymers. *J. Pharm. Pharmacol*. **53**: 303–315

Forster, A., Hempenstall, J., Tucker, I., Rades, T. (2001b) Selection of excipients for melt extrusion with two poorly water-soluble drugs by solubility parameter calculation and thermal analysis. *Int. J. Pharm*. **226**: 147–161

Forster, A., Hempenstall, J., Tucker, I., Rades, T. (2001c) The potential of small-scale fusion experiments and the Gordon-Taylor equation to predict the suitability of drug/polymer blends for melt extrusion. *Drug Dev. Ind. Pharm*. **27**: 549–560

Frisch, M. J., Trucks, G. W., Schlegel, H. B., Scuseria, G. E., Robb, M. A. C., Montgomery, J., J. A., Vreven, T., Kudin, K. N., Burant, J. C., Millam, J. M., Iyengar, S. S., Tomasi, J., Barone, V., Mennucci, B., Cossi, M., Scalmani, G., Rega, N., Petersson, G. A., Nakatsuji, H., Hada, M., Ehara, M., Toyota, K., Fukuda, R., Hasegawa, J., Ishida, M., Nakajima, T., Honda, Y., Kitao, O., Nakai, H., Klene, M., Li, X., Knox, J. E., Hratchian, H. P., Cross, J. B., Bakken, V., Adamo, C., Jaramillo, J., Gomperts, R., Stratmann, R. E., Yazyev, O., Austin, A. J., Cammi, R., Pomelli, C., Ochterski, J. W., Ayala, P. Y., Morokuma, K., Voth, G. A., Salvador, P., Dannenberg, J. J., Zakrzewski, V. G., Dapprich, S., Daniels, A. D., Strain, M. C., Farkas, O., Malick, D. K., Rabuck, A. D., Raghavachari, K., Foresman, J. B., Ortiz, J. V., Cui, Q., Baboul, A. G., Clifford, S., Cioslowski, J., Stefanov, B. B., Liu, G., Liashenko, A., Piskorz, P., Komaromi, I., Martin, R. L., Fox, D. J., Keith, T., Al-Laham, M. A., Peng, C. Y., Nanayakkara, A., Challacombe, M., Gill, P. M. W., Johnson, B., Chen, W., Wong, M. W., Gonzalez, C., Pople, J. A. (2004) *Gaussian 03, Revision C.02*. Gaussian Inc., Wallingford, CT

Galdecki, Z., Glówka, M. (1976) Crystal and molecular structure of $\gamma$-form of 1-(p-chlorobenzooyl)-5-methoxy-2-methylindole-3-acetic acid. A comparison of results based on photographic data with previous results obtained by means of a single crystal diffractometer. *Roczniki Chemii* **50**: 1139–1147

Guirgis, G. A., Nashed, Y. E., Durig, J. R. (2000) Infrared and Raman spectra, conformational stability, barriers to internal rotation, normal-coordinate calculations and vibrational assignments for vinyl silyl bromide. *Spectrochim. Acta Part A Mol. Biomol. Spectrosc*. **56**: 1065–1078

Hancock, B. C. (2002) Disordered drug delivery: destiny, dynamics and the Deborah number. *J. Pharm. Pharmacol*. **54**: 737–746

Hancock, B. C., Parks, M. (2000) What is the true solubility advantage for amorphous pharmaceuticals? *Pharm. Res*. **17**: 397–404

Kirstenmacher, T. J., Marsh, R. E. (1972) Crystal and molecular structure of an antiinflammatory agent, indomethacin, 1-(p-chlorobenzoyl)-5-methoxy-2-methylindole-3-acetic acid. *J. Am. Chem. Soc*. **94**: 1340–1345

Kubli-Garfias, C. (1998) Ab initio assessment of the electronic structure of 5 alpha-reduced progestins. *Int. J. Quant. Chem*. **67**: 329–338

Kubli-Garfias, C. (1999) Comparative study of the electronic structure of pregnanolones by ab initio theory. *Int. J. Quant. Chem*. **71**: 433–440

Martins, J. B. L., Perez, M. A., Silva, C. H. T. P., Taft, C. A., Arissawa, M., Longo, E., Mello, P. C., Stamato, F. M. L. G., Tostes, J. G. R. (2002) Theoretical ab initio study of ranitidine. *Int. J. Quant. Chem*. **90**: 575–586

Schaftenaar, G., Noordik, J. H. (2000) Molden: a pre- and post-processing program for molecular and electronic structures. *J. Comput. Aided Mol. Des*. **14**: 123–134

Scott, A. P., Radom, L. (1996) Harmonic vibrational frequencies: an evaluation of Hartree-Fock, Moller-Plesset, quadratic configuration interaction, density functional theory, and semiempirical scale factors. *J. Phys. Chem*. **100**: 16502–16513

Strachan, C. J., Howell, S. L., Rades, T., Gordon, K. C. (2004) A theoretical and spectroscopic study of carbamazepine polymorphs. *J. Raman Spectrosc*. **35**: 401–408

Taylor, L. S., Zografi, G. (1997) Spectroscopic characterization of interactions between PVP and indomethacin in amorphous molecular dispersions. *Pharm. Res*. **14**: 1691–1697

Taylor, L. S., Zografi, G. (1998) The quantitative analysis of crystallinity using FT-Raman spectroscopy. *Pharm. Res*. **15**: 755–761

Tong, P., Zografi, G. (2001) A study of amorphous molecular dispersions of indomethacin and its sodium salt. *J. Pharm. Sci*. **90**: 1991–2004

US Department of Health and Human Services, FDA, Center for Drug Evaluation and Research (CDER) (2000) Guidance for industry: waiver of in vivo bioavailability and bioequivalence studies for immediate-release solid oral dosage forms based on a biopharmaceutics classification system. http://www.fda.gov/cder/guidance/3618fnl.pdf (accessed 7 April 2003)

Watanabe, T., Wakiyama, N., Usui, F., Ikeda, M., Isobe, T., Senna, M. (2001) Stability of amorphous indomethacin compounded with silica. *Int. J. Pharm*. **226**: 81–91

Watanabe, T., Ohno, I., Wakiyama, N., Kusai, A., Senna, M. (2002) Stabilization of amorphous indomethacin by co-grinding in a ternary mixture. *Int. J. Pharm*. **241**: 103–111

Watanabe, T., Hasegawa, S., Wakiyama, N., Kusai, A., Senna, M. (2003) Comparison between polyvinylpyrrolidone and silica nanoparticles as carriers for indomethacin in a solid state dispersion. *Int. J. Pharm*. **250**: 283–286